

**DEVELOPMENT AND CHARACTERISATION OF  
ELECTROSPUN SOLID DISPERSIONS OF  
ATOVAQUONE FOR ENHANCED BUCCAL  
DRUG DELIVERY**

**TEOH XIN YI**

**UNIVERSITI SAINS MALAYSIA**

**2023**

**DEVELOPMENT AND CHARACTERISATION OF  
ELECTROSPUN SOLID DISPERSIONS OF  
ATOVAQUONE FOR ENHANCED BUCCAL  
DRUG DELIVERY**

by

**TEOH XIN YI**

**Thesis submitted in fulfilment of the requirements  
for the degree of  
Doctor of Philosophy**

**February 2023**

## ACKNOWLEDGEMENT

First of all, I would like to express my sincere gratitude to my supervisors Assoc Prof Dr Chan Siok Yee and Dr Goh Choon Fu for their continuous support, guidance, understanding and motivation throughout this project and thesis writing. Without their assistance and dedicated involvement, this thesis would have never been accomplished. Besides, many thanks to Emeritus Prof Dr Yuen Kah Hay, Dr Sherlyn Lim Sheau Chin and Dr Fung Wai Yee for their support in providing the electrospinning instrumentation accessibility and invaluable input to this project.

I am glad to have my colleagues and friends Ms Yeoh Yuyu, Mr Teh Chye Teik, Ms Yoong Lai Keng, Dr Nafiu Aminu, Dr Nasir Hayat Khan, Mr Edward Tan Kong Weng, Ms Wong Li Ching, Ms Reem Abou Assi, Mr Low Khai Hang, Mr Ooi Yen Hoe, Ms Toh Yee Han, Ms Chong Yong Chin, Mr Fong Tze Hung, Mr Khong Zhao Peng, Mr Hwang Jia Le, Dr Lee You Zhuan, Mr Seow Eng Kwong, Ms Elaine Lee, Ms Lee Wey Myn and Ms Yeoh Soo Chin for being an integral part of my postgraduate journey.

Besides, I am very grateful to my supervisor Dr Chan for providing an attachment opportunity to Prof Sheng Qi's group at the University of East Anglia. Guidance from Prof Sheng Qi and Emeritus Prof Peter Belton throughout the visit is fruitful and highly appreciated. Also, I would like to thank my friends who shared precious memories with me at UEA: Dr Yan Fen Lee, Dr Bin Zhang, Mr Chak Hin Tam, Ms Valeria Tamburrini, Mr Thomas McDonagh, Mr Sherif Hamdallah, Ms Damilola Ajulo, Ms Sandra Lazauskaite and Ms Pattaraporn Panraksa.

Last but not the least, my love and deepest appreciation to my family, Mr Teoh Khee Hua, Mrs Ng Guat Hoon and Mr Teoh Zhen Pei who have given me outstanding support and unconditional love throughout my life.

## TABLE OF CONTENTS

<b>ACKNOWLEDGEMENT</b> .....	<b>ii</b>
<b>TABLE OF CONTENTS</b> .....	<b>iii</b>
<b>LIST OF TABLES</b> .....	<b>xi</b>
<b>LIST OF FIGURES</b> .....	<b>xv</b>
<b>LIST OF SYMBOLS AND ABBREVIATIONS</b> .....	<b>xxiii</b>
<b>LIST OF APPENDICES</b> .....	<b>xxv</b>
<b>ABSTRAK</b> .....	<b>xxvi</b>
<b>ABSTRACT</b> .....	<b>xxviii</b>
<b>CHAPTER 1 INTRODUCTION AND LITERATURE REVIEW</b> .....	<b>1</b>
1.1 General Introduction .....	1
1.2 Atovaquone .....	3
1.2.1 Safety and Toxicity .....	4
1.2.2 Pharmacokinetics Profile.....	4
1.3 Solid-State Forms .....	5
1.3.1 Crystalline Materials .....	6
1.3.1(a) Polymorphism.....	7
1.3.1(b) Thermodynamic Stability of Polymorphs.....	9
1.3.1(c) Polymorph Conversion .....	12
1.3.2 Amorphous Materials.....	13
1.3.2(a) Formation of Amorphous Solids .....	14
1.3.2(b) Preparation of Amorphous Solids.....	15
1.3.2(c) Glass Transition Temperature.....	17
1.3.2(d) Fragility.....	18
1.4 Solid Dispersion .....	20
1.4.1 Classification of Solid Dispersion.....	23

1.4.1(a)	First Generation of Solid Dispersion .....	23
1.4.1(b)	Second Generation of Solid Dispersion.....	23
1.4.1(c)	Third Generation of Solid Dispersion.....	24
1.4.1(d)	Fourth Generation of Solid Dispersion.....	24
1.4.2	Types of Solid Dispersion .....	24
1.4.2(a)	Non-molecular Dispersion.....	25
1.4.2(b)	Molecular Dispersion.....	25
1.4.3	Thermodynamic Stability of Molecular Dispersion.....	26
1.4.3(a)	Theoretical Miscibility Estimation of Drug and Polymer.....	26
1.4.3(b)	Glass Transition Temperature.....	28
1.4.3(c)	Interaction of Drug and Polymer .....	28
1.4.4	Preparation Method for Solid Dispersion.....	29
1.4.4(a)	Kneading.....	29
1.4.4(b)	Melting.....	30
1.4.4(c)	Solvent Removal.....	31
1.4.4(d)	Melting Solvent .....	32
1.4.5	Advantages of Solid Dispersion.....	32
1.4.6	Limitations of Solid Dispersion .....	33
1.5	Electrospinning.....	33
1.5.1	History and Principle of Electrospinning.....	34
1.5.2	Parameters Affecting Electrospinning .....	38
1.5.2(a)	Solution Parameters .....	38
1.5.2(b)	Process Parameters .....	40
1.5.2(c)	Ambient Parameters.....	42
1.5.3	Application of Electrospinning in Commercial Products .....	43
1.5.4	Application of Electrospinning for Drug Delivery .....	48
1.5.4(a)	Oral Related Drug Delivery.....	50

1.5.4(b)	Non-oral Related Drug Delivery .....	56
1.5.5	Upscaling and Mass Production of Electrospun Fibres .....	65
1.5.5(a)	Nozzle-type Electrospinning .....	65
1.5.5(b)	Free Surface Electrospinning.....	67
1.6	Problem Statement .....	70
1.7	Rationale of Study.....	71
1.8	Scope of Study .....	73
<b>CHAPTER 2 MATERIALS AND METHODS .....</b>		<b>74</b>
2.1	Introduction .....	74
2.2	Materials.....	74
2.2.1	Carriers .....	74
2.2.1(a)	Homopolymer PVP.....	74
2.2.1(b)	Copolymer PVPVA .....	78
2.3	Electrospinning Setup .....	80
2.4	Characterisation Techniques .....	81
2.4.1	Thermogravimetric Analysis.....	81
2.4.2	Scanning Electron Microscopy .....	83
2.4.3	Attenuated Total Reflectance-Fourier Transform Infrared Spectroscopy .....	83
2.4.4	X-ray Powder Diffraction.....	85
2.4.5	Single Crystal X-Ray Diffraction.....	86
2.4.6	Differential Scanning Calorimetry.....	87
2.5	Drug Release Study.....	89
2.6	Permeation Study .....	94
2.7	Concluding Remarks .....	96
<b>CHAPTER 3 SOLID CHARACTERISATION OF ATOVAQUONE.....</b>		<b>97</b>
3.1	Introduction .....	97
3.2	Methodology .....	99

3.2.1	Materials.....	99
3.2.2	Sample Preparation .....	100
	3.2.2(a) Thermal Treatment on Atovaquone.....	100
	3.2.2(b) Sublimation of Atovaquone.....	100
	3.2.2(c) Evaporation of Atovaquone.....	100
	3.2.2(d) Quench cooling of Atovaquone.....	101
3.2.3	Drug Content Assay .....	101
3.2.4	Characterisation Techniques .....	101
	3.2.4(a) Thermogravimetric Analysis .....	101
	3.2.4(b) Scanning Electron Microscopy.....	102
	3.2.4(c) Attenuated Total Reflectance-Fourier Transform Infrared Spectroscopy .....	102
	3.2.4(d) X-ray Powder Diffraction.....	103
	3.2.4(e) Single Crystal X-Ray Diffraction .....	103
	3.2.4(f) Differential Scanning Calorimetry .....	104
3.2.5	Fragility Calculation.....	105
3.2.6	Saturated Solubility.....	105
3.2.7	Statistical Analysis .....	106
3.3	Results .....	106
	3.3.1 Thermal Treatment and Drug Content Assay .....	106
	3.3.2 Thermogravimetric Analysis.....	109
	3.3.3 Scanning Electron Microscopy .....	111
	3.3.4 Attenuated Total Reflectance-Fourier Transform Infrared Spectroscopy .....	112
	3.3.5 X-ray Powder Diffraction.....	114
	3.3.6 Single Crystal X-Ray Diffraction.....	116
	3.3.7 Differential Scanning Calorimetry .....	122
	3.3.8 Fragility Calculation.....	127

3.3.9	Saturated Solubility .....	130
3.4	Discussion .....	130
3.5	Conclusion.....	133
<b>CHAPTER 4 OPTIMISATION AND CHARACTERISATION OF ELECTROSPINNING OF ATOVAQUONE SOLID DISPERSION.....</b>		<b>134</b>
4.1	Introduction .....	134
4.2	Methodology .....	136
4.2.1	Materials.....	136
4.2.2	Theoretical Miscibility Estimation of Drug and Polymer .....	137
4.2.3	Theoretical Estimation of Glass Transition Temperature .....	138
4.2.4	Sample Preparation .....	139
4.2.5	Viscosity.....	141
4.2.6	Moisture Content.....	141
4.2.7	Drug Content Assay .....	141
4.2.8	Characterisation Techniques .....	142
4.2.8(a)	Attenuated Total Reflectance-Fourier Transform Infrared Spectroscopy .....	142
4.2.8(b)	Light Microscopy.....	142
4.2.8(c)	Differential Scanning Calorimetry .....	142
4.2.8(d)	X-ray Powder Diffraction.....	143
4.2.8(e)	Scanning Electron Microscopy.....	143
4.2.9	Statistical Analysis .....	143
4.3	Results .....	144
4.3.1	Theoretical Miscibility Estimation of Drug and Polymer .....	144
4.3.2	Theoretical Estimation of Glass Transition Temperature .....	146
4.3.3	Sample Preparation and Optimisation.....	148
4.3.4	Viscosity.....	153
4.3.5	Moisture Content.....	155



4.3.6	Drug Content Assay .....	157
4.3.7	Attenuated Total Reflectance-Fourier Transform Infrared Spectroscopy .....	157
4.3.8	Light Microscopy .....	160
4.3.9	Differential Scanning Calorimetry .....	162
4.3.10	X-ray Powder Diffraction.....	167
4.3.11	Scanning Electron Microscopy .....	169
4.4	Discussion .....	171
4.5	Conclusion.....	173
<b>CHAPTER 5 IN VITRO AND EX VIVO EVALUATION OF ATOVAQUONE ELECTROSPUN FIBRES FOR BUCCAL DRUG DELIVERY .....</b>		<b>174</b>
5.1	Introduction .....	174
5.2	Methodology .....	177
5.2.1	Materials.....	177
5.2.2	Sample Preparation .....	178
5.2.3	<i>In vitro</i> Evaluation.....	178
	5.2.3(a) Saturated Solubility Study .....	178
	5.2.3(b) Drug Release Study .....	178
5.2.4	<i>Ex vivo</i> Evaluation.....	180
	5.2.4(a) Preparation of Porcine Buccal Membrane.....	180
	5.2.4(b) Permeation Study.....	180
5.2.5	Statistical Analysis .....	182
5.3	Results .....	182
5.3.1	Saturated Solubility Study.....	182
5.3.2	Drug Release Study.....	184
5.3.3	Permeation Study .....	192
5.4	Discussion .....	199

5.5	Conclusion.....	204
<b>CHAPTER 6 STORAGE STABILITY OF ATOVAQUONE</b>		
<b>ELECTROSPUN FIBRES ..... 205</b>		
6.1	Introduction .....	205
6.2	Methodology .....	207
6.2.1	Materials.....	207
6.2.2	Sample Preparation .....	208
6.2.3	Accelerated Condition.....	208
6.2.3(a)	Storage Condition .....	208
6.2.3(b)	Light Microscopy.....	208
6.2.3(c)	Drug Content Assay.....	209
6.2.3(d)	Drug Release Study .....	209
6.2.4	Dry and Normal Room Temperature Condition .....	209
6.2.4(a)	Storage Condition .....	209
6.2.4(b)	Drug Content Assay.....	209
6.2.4(c)	Attenuated Total Reflectance-Fourier Transform Infrared Spectroscopy .....	210
6.2.4(d)	Differential Scanning Calorimetry .....	210
6.2.4(e)	Drug Release Study .....	210
6.2.5	Statistical Analysis .....	211
6.3	Results .....	211
6.3.1	Accelerated Condition.....	211
6.3.1(a)	Light Microscopy.....	212
6.3.1(b)	Drug Content Assay.....	220
6.3.1(c)	Drug Release Study .....	222
6.3.2	Dry and Normal Room Temperature Condition .....	229
6.3.2(a)	Drug Content Assay.....	229

6.3.2(b)	Attenuated Total Reflectance-Fourier Transform Infrared Spectroscopy .....	232
6.3.2(c)	Differential Scanning Calorimetry .....	235
6.3.2(d)	Drug Release Study .....	237
6.4	Discussion .....	242
6.5	Conclusion.....	247
<b>CHAPTER 7 CONCLUSION AND FUTURE WORK .....</b>		<b>249</b>
7.1	General Conclusion .....	249
7.2	Recommendations for Future Work.....	252
<b>REFERENCES.....</b>		<b>255</b>
<b>APPENDICES</b>		
<b>LIST OF PUBLICATIONS</b>		
<b>CONFERENCE ATTENDANCE</b>		

## LIST OF TABLES

	<b>Page</b>
Table 1.1	Biopharmaceutics Classification System of API according to aqueous solubility and intestinal permeability.....2
Table 1.2	Physicochemical properties of ATQ .....4
Table 1.3	Physical properties variation in polymorphs (Byrn et al., 2017b) .....9
Table 1.4	Preparation of amorphous solids (Byrn et al., 2017a, Newman, 2015) ..... 16
Table 1.5	Commercially available FDA-approved solid dispersion products ...21
Table 1.6	Commercial products by electrospinning technology.....44
Table 1.7	Clinical trials of electrospinning application (ClinicalTrials.gov, 2022) .....49
Table 1.8	Electrospinning research on oral related drug delivery.....50
Table 1.9	Electrospinning research on non-oral related drug delivery .....56
Table 2.1	Soluble grades of PVP available in the market..... 76
Table 2.2	Specifications of soluble PVPVA 64 ..... 79
Table 2.3	FDA-recommended dissolution method for ASD-based product. This table is adapted from Sun et al. (Sun et al., 2016) .....91
Table 3.1	Details of material used in the current study.....99
Table 3.2	Content recovery percentage of ATQ heated at specified temperatures isotherm for 30 minutes, n = 3 ..... 108
Table 3.3	Crystal data and data collection parameters of ATQ species..... 117
Table 3.4	Potential hydrogen bonding interactions (Å, °) of ATQ species ..... 121
Table 3.5	Fragility index estimation of quench cooled ATQ..... 128
Table 3.6	Analysis of independent samples t-test on the saturated solubility of raw ATQ and evaporated ATQ at room temperature, n = 3 ..... 130

Table 4.1	Details of material used in the current study.....	136
Table 4.2	Electrospinning parameters utilised for sample production.....	140
Table 4.3	Solubility parameter component group contribution calculation of ATQ based on the Hoftyzer-Van Krevelen method.....	144
Table 4.4	Solubility parameter of drug and polymeric carriers .....	145
Table 4.5	Theoretical glass transition temperature of ATQ electrospun systems estimated using the Gordon-Taylor equation .....	147
Table 4.6	Optimisation of electrospinning parameters including polymer blend ratio and voltage applied .....	151
Table 4.7	Analysis of independent samples t-test on the work of cohesion of electrospinning solution, n = 3 .....	154
Table 4.8	Analysis of independent samples t-test on the moisture content of blank electrospun samples, n = 3 .....	156
Table 4.9	Percentage of recovery of electrospun samples, n = 3 .....	157
Table 5.1	Details of material used in the current study.....	177
Table 5.2	Saturated solubility of raw ATQ and electrospun samples in distilled water at room temperature, n = 3 .....	182
Table 5.3	Saturated solubility of ATQ at 37°C, n = 3.....	183
Table 5.4	Initial drug release rate of samples in the first 30 minutes, n = 3 ....	186
Table 5.5	Specific pairwise comparison of the initial drug release rate of samples in the first 30 minutes analysed using ANOVA, n = 3 .....	187
Table 5.6	Specific pairwise comparison of the percentage of released between raw ATQ and electrospun systems analysed using ANOVA, n = 3 .....	190
Table 5.7	Permeation performance of raw ATQ, physical mixtures and electrospun samples, $3 \leq n \leq 4$ .....	194
Table 5.8	Specific pairwise comparison of the concentration permeated between raw ATQ and electrospun systems analysed using ANOVA, $3 \leq n \leq 4$ .....	197

Table 5.9	Specific pairwise comparison of flux between raw ATQ, physical mixtures and electrospun systems analysed using ANOVA, $3 \leq n \leq 4$ .....	197
Table 6.1	Details of material used in the current study.....	207
Table 6.2	Analysis of independent samples t-test on the recovery of electrospun samples upon storage in $75 \pm 5\%$ RH and $40 \pm 2^\circ\text{C}$ conditions for 3 months, $n = 3$ .....	221
Table 6.3	Specific pairwise comparison of the percentage of released between raw ATQ and electrospun samples after storage in the accelerated condition ( $75 \pm 5\%$ RH, $40 \pm 2^\circ\text{C}$ ) analysed using ANOVA, $n = 3$ .....	224
Table 6.4	Specific pairwise comparison of the percentage of released between electrospun samples after 2 and 3 months of storage in the accelerated condition ( $75 \pm 5\%$ RH, $40 \pm 2^\circ\text{C}$ ) analysed using ANOVA, $n = 3$ .....	226
Table 6.5	Analysis of independent samples t-test on the recovery of electrospun samples upon storage in $0\%$ RH and $25 \pm 2^\circ\text{C}$ conditions for 12 months, $n = 3$ .....	231
Table 6.6	Changes of carbonyl peak around $1600\text{-}1700\text{ cm}^{-1}$ of electrospun samples after 12 months of storage in $0\%$ RH and $25 \pm 2^\circ\text{C}$ conditions .....	234
Table 6.7	Changes in the glass transition temperature of electrospun samples after 12 months of storage in $0\%$ RH and $25 \pm 2^\circ\text{C}$ conditions.....	236
Table 6.8	Specific pairwise comparison of the percentage of released between raw ATQ and electrospun samples after 12 months of storage in dry and temperate conditions ( $0\%$ RH, $25 \pm 2^\circ\text{C}$ ) analysed using ANOVA, $n = 3$ .....	239
Table 6.9	Specific pairwise comparison of the percentage of released between freshly prepared electrospun samples and electrospun samples after 12 months of storage in dry and temperate conditions ( $0\%$ RH, $25 \pm 2^\circ\text{C}$ ) analysed using ANOVA, $n = 3$ .....	242

Table i	Details of material used in the current study.....	317
Table ii	Details of instruments used in the current study .....	318
Table iii	Details of chromatographic conditions applied in this study .....	318
Table iv	Linearity, detection limit and quantitation limit values .....	322
Table v	Accuracy and precision values .....	323
Table vi	Robustness data.....	324
Table vii	The compilation of ATQ polymorphs preparation methods .....	328

## LIST OF FIGURES

	<b>Page</b>
Figure 1.1	Molecular structure of ATQ.....3
Figure 1.2	Schematic illustration of different states of solid material. This figure is adapted from Hilfiker et al. (Hilfiker et al., 2006).....6
Figure 1.3	Relationship between Gibbs free energy and temperature for monotropic and enantiotropic polymorph pair. This figure is adapted and modified from Byrn et al. (Byrn et al., 2017b) ..... 10
Figure 1.4	(A) Plot of Gibbs free energy against the temperature of a material at its respective equilibrium and non-equilibrium states. This figure is adapted and modified from Byrn et al. (Byrn et al., 2017a). (B) Plot of enthalpy and volume against the temperature of a material at its respective state transition (crystallization or glass transition). This figure is adapted and modified from Reading and Craig (Reading and Craig, 2007) ..... 15
Figure 1.5	Simplified fragility schematic plot defined by Angell (Angell, 1995) ..... 18
Figure 1.6	Types of molecular dispersion, i.e., crystalline and amorphous. The solute molecules are highlighted in black. This figure is adapted and modified from Leuner and Dressman (Leuner and Dressman, 2000). .....26
Figure 1.7	Summary of preparation method for solid dispersion.....29
Figure 1.8	Schematic diagram of electrospinning horizontal setup .....35
Figure 1.9	Schematic drawing of the droplet deformation in electrospinning, (A) pendant drop, no droplet deformation, (B) charge accumulation on the droplet when low voltage is applied, (C) Coulombic repulsion over droplet surface tension, deformation of the droplet into Taylor cone and (D) jet formation from the Taylor cone when high voltage is applied. The figures are adapted and



	modified from Suresh et al. and Singh and Subramanian (Suresh et al., 2020, Singh and Subramanian, 2020) .....	36
Figure 1.10	Schematic drawing of jet bending instability. This figure is adapted and modified from Reneker and Yarin (Reneker and Yarin, 2008)...	37
Figure 1.11	Summary of parameters affecting the electrospinning process.....	38
Figure 1.12	Summary of nozzle-type electrospinning: (A) linear multi-needle, (B) square/rectangular arrangement multi-needle, (C) concentric configuration multi-needle, (D) hexagon with equilateral triangle organisation multi-needle, (E) flat, (F) porous tube, (G) electroblowing/blow-assisted, (H) air-stream-assisted and (I) nozzle-based high-speed (rotary). This figure is adapted and modified from Vass et al. (Vass et al., 2019b).....	66
Figure 1.13	Summary of stationary free surface electrospinning method: (A) conical wire, (B) curved slot, (C) slit, (D) wire, (E) plate edge, (F) bowl and (G) stepped pyramid. This figure is adapted and modified from Vass et al. (Vass et al., 2019b) .....	68
Figure 1.14	Summary of moving free surface electrospinning method: (A) magnetic fluid, (B) corona, (C) free surface high-speed, (D) beaded-chain (E) bubble, (F) ball, (G) rotary disk, (H) spiral coil, (I) rotary wire and (J) cylinder. This figure is adapted and modified from Vass et al. (Vass et al., 2019b) .....	69
Figure 2.1	Molecular structure of PVP monomer .....	75
Figure 2.2	Molecular structure of PVPVA monomer .....	78
Figure 2.3	Diagram of (A) electrospinning setup and (B) stable Taylor cone jet.....	81
Figure 2.4	Schematic diagram of TGA instrument. This figure is adapted and modified from (Ogata et al., 2004).....	82
Figure 2.5	Illustration of an evanescent wave resulting from total internal reflection. This figure is adapted and modified from (AntonPaar, 2022) .....	84

Figure 2.6	Illustration of simple scattering based on Bragg's law condition. This figure is adapted from Stan et al (Stan et al., 2018).....	85
Figure 2.7	Schematic diagram of (A) power compensation DSC and (B) heat flux DSC. S and R indicate sample and reference respectively. This figure is adapted from Clas et al. (Clas et al., 1999).....	87
Figure 2.8	Drug release profile of ASD under non-sink dissolution condition with sink index (A) 3.56 (close to perfect sink), (B) 0.533 (intermediate non-sink) and (C) 0.136 (extremely non-sink). The dashed line represents the equilibrium solubility of crystalline API in its respective dissolution medium. This figure is adapted and modified from Van Speybroeck et al. and Sun et al. (Van Speybroeck et al., 2010, Sun et al., 2016).....	93
Figure 2.9	Schematic diagram of (A) Ussing chamber and (B) standard Franz diffusion cell. This figure is adapted and modified from Puckrin and PermeGear (Puckrin, 2020, PermeGear, 2019).....	95
Figure 3.1	Physical observation of (A1) ATQ heated at 200°C in petri dish, (A2) products formed at petri dish cover after isothermal heating at 200°C for an hour, (B1) ATQ heated at 230°C in petri dish and (B2) products formed at petri dish cover after isothermal heating at 230°C.....	107
Figure 3.2	Physical observation of ATQ after heating at specified temperatures ranged 180-330°C.....	108
Figure 3.3	TGA profile of ATQ .....	110
Figure 3.4	SEM images for (A) raw ATQ, (B) sublimated ATQ, (C) evaporated ATQ and (D) quench cooled ATQ .....	111
Figure 3.5	FTIR spectra of (A) sublimated ATQ, (B) evaporated ATQ, (C) quench cooled ATQ and (D) raw ATQ.....	113
Figure 3.6	XRPD spectra for (A) sublimated ATQ, (B) evaporated ATQ, (C) quench cooled ATQ and (D) raw ATQ.....	115
Figure 3.7	Schematic drawing of the crystal packing of (A) Ato-II, (B) Ato-III and (C) Ato-eva. Structures of Ato-II and Ato-III were	

	reproduced from Nayak et al. and Malpezzi et al., respectively (Malpezzi et al., 2010, Nayak et al., 2013). Dashed circles and atoms highlighted in yellow indicate the structural arrangement difference in Ato-eva compared Ato-III .....	119
Figure 3.8	Molecular structure of Ato-eva with the same atom-labelling as polymorphs adapted from literature (Malpezzi et al., 2010). H-atoms highlighted in yellow indicate the structural arrangement difference in Ato-eva compared Ato-III .....	120
Figure 3.9	DSC thermograms of raw ATQ with repeated heat-cool-heat cycles.....	123
Figure 3.10	Formation of sublimated ATQ traces on DSC furnace lid.....	124
Figure 3.11	DSC thermograms of (A) raw ATQ, (B) sublimated ATQ and (C) evaporated ATQ.....	125
Figure 3.12	DSC thermograms of quench cooled ATQ, n = 5.....	126
Figure 3.13	Heating rate dependence of the putative $T_g$ of quench cooled ATQ, $2 \leq n \leq 5$ .....	127
Figure 3.14	Summary of solid form changes of ATQ form I in this study. Form II (Nayak et al., 2013) was excluded as it was not observed as part of the outcomes of this study. ....	132
Figure 4.1	Morphology of (A) ES ATQ/VA, (B) ES ATQ/VA:K90 1:1, (C) ES ATQ/VA:K90 1:3, (D) ES ATQ/VA:K90 1:5 and (E) ES ATQ/K90 with fixed processing voltage at 12 kV and 20 kV; observed under magnification of (1) 1000 $\times$ and (2) 5000 $\times$ . Arrows and circles indicate the beads within smooth fibres and fragments attached to smooth fibres .....	150
Figure 4.2	Collection of 10% w/w ATQ (A) electrosprayed powder and (B) electrospun mat; 20 kV .....	152
Figure 4.3	Relationship between the amount of vinyl acetate by dry weight with the moisture content of freshly prepared electrospun samples, n = 3 .....	156

Figure 4.4	FTIR spectra of (A) raw ATQ, (B) dried PVPVA 64, (C) dried PVP K90, (D) ES ATQ/VA, (E) ES ATQ/VA:K90 1:1, (F) ES ATQ/VA:K90 1:3, (G) ES ATQ/VA:K90 1:5 and (H) ES ATQ/K90 .....	158
Figure 4.5	Morphology of (A) raw ATQ, (B) ES ATQ/VA, (C) ES ATQ/VA:K90 1:1, (D) ES ATQ/VA:K90 1:3, (E) ES ATQ/VA:K90 1:5 and (F) ES ATQ/K90 under (1) non-polarised light and (2) polarised light microscopy .....	161
Figure 4.6	DSC thermograms of (A) raw ATQ, (B) PVPVA 64, (C) PVP K90, (D) ES ATQ/VA, (E) ES ATQ/VA:K90 1:1, (F) ES ATQ/VA:K90 1:3, (G) ES ATQ/VA:K90 1:5 and (H) ES ATQ/K90.....	163
Figure 4.7	Comparison of the experimental and theoretical glass transition temperature of electrospun systems predicted using the Gordon-Taylor equation .....	165
Figure 4.8	XRPD spectra of (A) raw ATQ, (B) PM ATQ/VA:K90 1:1, (C) PM ATQ/K90, (D) ES ATQ/VA, (E) ES ATQ/VA:K90 1:1, (F) ES ATQ/VA:K90 1:3, (G) ES ATQ/VA:K90 1:5 and (H) ES ATQ/K90 .....	168
Figure 4.9	Diameter distribution plots of (A) ES ATQ/VA:K90 1:1, (B) ES ATQ/VA:K90 1:3, (C) ES ATQ/VA:K90 1:5 and (D) ES ATQ/K90, n = 100 .....	170
Figure 5.1	Drug release profile of raw ATQ (●), physical mixture (▲) and electrospun samples (■), n = 3 .....	185
Figure 5.2	Drug release profile of raw ATQ (●), ES ATQ/VA (▲), ES ATQ/VA:K90 1:1 (■), ES ATQ/VA:K90 1:3 (×), ES ATQ/VA:K90 1:5 (◆) and ES ATQ/K90 (○) over (A) 30 minutes and (B) 120 minutes, n = 3.....	188
Figure 5.3	Relationship between the amount of vinyl acetate by dry weight with the occurrence of precipitation.....	189

Figure 5.4	Physical observation of dissolution medium at the end of the study of (A) ES ATQ/VA and (B) ES ATQ/K90.....	191
Figure 5.5	Physical observation of the orange intensity reduction and recrystallisation of ATQ in the remaining dissolution medium when it was brought to cool at room temperature (A) immediately, after (B) 2 hours, (C) 4 hours and (D) 24 hours end of drug release study.....	192
Figure 5.6	Permeation profile of raw ATQ (●), physical mixture (▲) and electrospun samples (■), n = 3 .....	193
Figure 5.7	Permeation profile of ATQ (●), ES ATQ/VA (▲), ES ATQ/VA:K90 1:1 (■), ES ATQ/VA:K90 1:3 (×), ES ATQ/VA:K90 1:5 (◆) and ES ATQ/K90 (○), $3 \leq n \leq 4$ .....	196
Figure 5.8	Proposed mechanism of the maintenance of ATQ supersaturation by the hydrophobic vinyl acetate component of the polymer matrix in ES ATQ/VA:K90 1:1 (upper panel) and recrystallisation in ES ATQ/K90 (lower panel) during the dissolution process. The dashed line indicates the onset of observed precipitates on the surface of the dissolution medium .....	202
Figure 6.1	Morphology of (A) ES ATQ/VA, (B) ES ATQ/VA:K90 1:1, (C) ES ATQ/VA:K90 1:3, (D) ES ATQ/VA:K90 1:5 and (E) ES ATQ/K90 under non-polarised light microscopy up to 3 months storage in an accelerated condition ( $75 \pm 5\%$ RH, $40 \pm 2^\circ\text{C}$ ).....	213
Figure 6.2	Morphology of (A) ES ATQ/VA, (B) ES ATQ/VA:K90 1:1, (C) ES ATQ/VA:K90 1:3, (D) ES ATQ/VA:K90 1:5 and (E) ES ATQ/K90 under polarised light microscopy up to 3 months storage in an accelerated condition ( $75 \pm 5\%$ RH, $40 \pm 2^\circ\text{C}$ ).....	216
Figure 6.3	Change in intensity of polarised light microscopy image of ES ATQ/VA (▲), ES ATQ/VA:K90 1:1 (■), ES ATQ/VA:K90 1:3 (×), ES ATQ/VA:K90 1:5 (◆) and ES ATQ/K90 (○) over time.....	218

Figure 6.4	Physical observation of the colour of (A) freshly prepared electrospayed powder, (B) electrospayed powder after 3 months of storage in the accelerated condition ( $75 \pm 5\%$ RH, $40 \pm 2^\circ\text{C}$ ); (C) freshly prepared electrospun fibres and (D) electrospun fibres after 3 months storage in the accelerated condition ( $75 \pm 5\%$ RH, $40 \pm 2^\circ\text{C}$ ).....	220
Figure 6.5	Drug release profile of raw ATQ (●), freshly prepared electrospun samples (▲) and electrospun samples stored in $75 \pm 5\%$ RH and $40 \pm 2^\circ\text{C}$ for 2 months (■) and 3 months (×), n = 3 .....	223
Figure 6.6	Drug release profile of raw ATQ (●); ES ATQ/VA (▲), ES ATQ/VA:K90 1:1 (■), ES ATQ/VA:K90 1:3 (×), ES ATQ/VA:K90 1:5 (◆) and ES ATQ/K90 (○) after storage in $75 \pm 5\%$ RH and $40 \pm 2^\circ\text{C}$ for (A) 3 months and (B) 3 months with 25% sample weight reduction correction based on the average drug recovery from 3-months aged electrospun samples, n = 3.....	228
Figure 6.7	Physical observation of the colour of (A) freshly prepared electrospayed powder, (B) electrospayed powder after 12 months of storage in 0% RH and $25 \pm 2^\circ\text{C}$ ; (C) freshly prepared electrospun fibres and (D) electrospun fibres after 12 months storage in 0% RH and $25 \pm 2^\circ\text{C}$ conditions .....	229
Figure 6.8	FTIR spectra of (A) ES ATQ/VA, (B) ES ATQ/VA:K90 1:1, (C) ES ATQ/VA:K90 1:3, (D) ES ATQ/VA:K90 1:5 and (E) ES ATQ/K90 after 12 months storage in 0% RH and $25 \pm 2^\circ\text{C}$ conditions .....	233
Figure 6.9	DSC thermograms of (A) ES ATQ/VA, (B) ES ATQ/VA:K90 1:1, (C) ES ATQ/VA:K90 1:3, (D) ES ATQ/VA:K90 1:5 and (E) ES ATQ/K90 after 12 months storage in 0% RH and $25 \pm 2^\circ\text{C}$ conditions .....	236
Figure 6.10	Drug release profile of raw ATQ (●); ES ATQ/VA (▲), ES ATQ/VA:K90 1:1 (■), ES ATQ/VA:K90 1:3 (×), ES	

	ATQ/VA:K90 1:5 (◆) and ES ATQ/K90 (○) after storage in 0% RH and 25 ± 2°C conditions for 12 months, n = 3.....	238
Figure 6.11	Drug release profile of raw ATQ (●), freshly prepared electrospun samples (▲) and electrospun samples after 12 months storage in 0% RH and 25 ± 2°C conditions (◆), n = 3 .....	241
Figure 6.12	Proposed mechanism of the maintenance of ATQ supersaturation by the annealing effect in the aged electrospun sample during the dissolution process. The amorphous structure undergoes structural relaxation towards the equilibrium state during the ageing process. A more pronounced stabilising effect through structural relaxation was observed in the system without a hydrophobic component (lower panel, ES ATQ/K90) than in the system with a hydrophobic component (upper panel, ES ATQ/VA:K90 1:1) as a hydrophobic component was proposed to show an initial stabilisation effect on the system.....	245
Figure i	Standard chromatogram of ATQ in methanol.....	320
Figure ii	Overlay chromatograms of (A) blank methanol, (B) methanol spiked with ATQ, (C) blank dissolution medium, (D) dissolution medium spiked with ATQ, (E) blank permeation medium after reaction with buccal skin and (F) permeation medium after reaction with buccal skin spiked with ATQ.....	321
Figure iii	Recrystallisation of ATQ (A) present in the non-pre-treated sample and (B) absent in the pre-treated sample after one-day storage in the screwed vial at room temperature .....	325
Figure iv	Recrystallisation of permeated (A) ES ATQ/VA and (B) ES ATQ/K90 upon 12 hours of storage in the screwed vial (without solvent dilution) observed under (1) non-polarised and (2) polarised light microscopy .....	327

## LIST OF SYMBOLS AND ABBREVIATIONS

%	Percent
/	Per
°	Degree
°C	Degree of Celsius
<	Less than
>	More than
µg	Microgram
µL	Microliter
µm	Micrometer
ACN	Acetonitrile
AD	Average diameter
ANOVA	Analysis of variance
API	Active pharmaceutical ingredient
ATQ	Atovaquone
ATR-FTIR	Attenuated total reflectance-Fourier transform infra-red
BCS	Biopharmaceutical classification system
cm	Centimetre
DE	Dissolution efficiency
DSC	Differential scanning calorimetry
ES	Electrospun
FDA	Food and drug administration
g	Gram
h	Hour
HME	Hot melt extrusion
HPC	Hydroxypropyl cellulose
HPLC	High performance liquid chromatography
HPMC	Hydroxypropyl methylcellulose
HPMC-AS	Hydroxypropyl methylcellulose acetate succinate
ICH	International conference on harmonization of technical requirements for registration of pharmaceuticals for human use
ID	Internal diameter
IPA	Iso-propyl alcohol



kV	Kilovolts
LC	Liquid chromatography
LOD	Limit of detection
LOQ	Limit of quantitation
M	Molar
mA	Milliampere
mL	Milliliter
mm	Millimeter
nm	Nanometer
PEG	Polyethylene glycol
PM	Physical mixture
PVP	Polyvinyl pyrrolidone
PVPVA	Polyvinyl pyrrolidone vinyl acetate
R <sup>2</sup>	Regression value
RH	Relative humidity
rpm	Rate per minute
RSD	Relative standard deviation
S.D.	Standard deviation
SCXR	Single crystal X-ray diffraction
SD	Solid dispersion
SEM	Scanning electron microscopy
SLS	Sodium lauryl sulphate
T <sub>g</sub>	Glass transition temperature
TPGS	D- $\alpha$ -Tocopherol polyethylene glycol succinate
UV	Ultraviolet
VA	Vinyl acetate
VP	Vinyl pyrrolidone
w/v	Weight-to-volume ratio
w/w	Weight-to-weight ratio
XRPD	X-ray powder diffraction

## LIST OF APPENDICES

- Appendix A      Development and Validation of a Simple High-Performance Liquid Chromatographic (HPLC) Analytical Method for Atovaquone Quantitation
- Appendix B      Polymorphs of Atovaquone

**PEMBANGUNAN DAN PENCIRIAN SEBARAN PEPEJAL  
ELEKTROPINTALAN ATOVAQUONE UNTUK MENINGKATKAN  
PENYAMPAIAN DRUG SECARA BUKAL**

**ABSTRAK**

Kajian ini menyiasat drug kurang larut air, atovaquone (ATQ) yang dirumus melalui strategi penyebaran pepejal elektropintalan bersama sistem pembawa polimer. Rawatan haba telah dikenakan pada ATQ polimorf I dan melaporkan sifat sensitif haba yang mana ATQ memejalwap sebelum suhu takat lebur. Polimorf baharu ATQ (ATQ polimorf sub/eva) telah dikesan hasil daripada pemejalwapan dan penyejatan rawatan haba tersebut. Kajian DSC menunjukkan suhu peralihan sekitar  $-20^{\circ}\text{C}$  yang dikesan melalui rawatan pelindapkejutan cair. Berikutan itu, teknik elektropintalan yang tidak melibatkan haba telah digunakan untuk menghasilkan sebaran pepejal ATQ bersama pembawa polimer PVPVA atau/dan PVP. Produk elektropintalan ATQ-polimer yang dihasilkan mempunyai kandungan ATQ yang tinggi telah dipulih melalui kaedah HPLC yang ditubuhkan dalam kajian ini. Analisis ATR-FTIR menunjukkan interaksi ikatan hidrogen antara ATQ dan polimer. Pengurangan hablur ATQ dalam produk selepas elektropintalan telah disahkan melalui XRPD. ATQ hasil elektropintalan turut menunjukkan peningkatan keterlarutan dan profil perlarutan drug berbanding hablur tulen ATQ. Keseimbangan hidrofilik-hidrofobik sistem polimer merupakan faktor utama dalam pengekalan perlarutan ATQ dalam medium dan menghalang penghabluran semula. Walaupun bersifat separa hablur, hasil elektropintalan yang terdiri daripada rumusan polimer (ES ATQ/VA:K90 1:1) menunjukkan peningkatan profil perlarutan yang berterusan. Manfaat pengekalan keseimbangan hidrofilik-hidrofobik sistem polimer turut mempengaruhi profil penyerapan drug. Campuran fizikal dan hasil elektropintalan ATQ/VA:K90 1:1 mengambil masa yang tersingkat

untuk penyerapan melalui kulit berbanding dengan rumusan polimer yang lain. Penyiasatan lanjut mengenai kestabilan fizikal menunjukkan produk elektropintalan ATQ-polimer berjaya mengekalkan sifat amorfus dalam keadaan yang kering pada suhu bilik. Penuaan hasil elektropintalan melalui penyimpanan dalam keadaan yang kering mengelakkan penghabluran semula akibat larutan. Situasi ini demikian kerana proses penuaan telah membenarkan penstabilan hasil elektropintalan yang bersifat amorfus melalui pengenduran struktur. Penuaan produk menunjukkan bahawa rumusan yang hanya mengandungi komponen hidrofilik dalam sistem pembawa (ES ATQ/K90) membawa faedah yang lebih nyata berbanding rumusan lain yang mengandungi komponen hidrofobik dalam pengekal ketepuan secara berlebihan dalam proses perlarutan. Hasil penemuan ini menjadi pengetahuan yang penting untuk mencapai keadaan pengekal ketepuan yang berlebihan semasa perlarutan oleh sebaran pepejal amorfus selain daripada pengekal keseimbangan hidrofilik-hidrofobik sistem pembawa polimer.

**DEVELOPMENT AND CHARACTERISATION OF ELECTROSPUN SOLID  
DISPERSIONS OF ATOVAQUONE FOR ENHANCED BUCCAL DRUG  
DELIVERY**

**ABSTRACT**

The present study investigated a poorly aqueous soluble drug, atovaquone (ATQ) formulated using an electrospinning solid dispersion strategy with polymer carrier systems. Thermal treatment was applied to ATQ form I and reported heat-sensitive properties where it sublimates and degrades before melting temperature. Following the thermal treatment, a new polymorph (ATQ form sub/eva) was obtained as a result of sublimation and evaporation. Besides, an anomalous stepwise transition circa -20°C was identified from the ATQ produced via melt-quenching demonstrating the possibility of ATQ amorphisation. Subsequently, a non-heat invasive electrospinning technique was utilised to produce solid dispersions of ATQ with the polymer PVPVA or/and PVP. High content recovery of ATQ electrospun samples was quantitated by a novel HPLC method developed herein. Hydrogen bonding interactions between ATQ and polymers were identified through ATR-FTIR analysis. A reduction of ATQ crystallinity was confirmed in the electrospun samples and the ATQ electrospun solid dispersions have been shown to improve the solubility and drug release profiles compared to the raw crystalline ATQ. However, there was no proportional relationship between the degree of crystallinity reduction and the improvement of the drug release profile reported. Instead, an optimisation of the hydrophilic-hydrophobic balance of the polymeric system was highlighted to sustain the supersaturation state by preventing solution-mediated recrystallisation of the electrospun samples. Despite being a partially crystalline system, the optimised polymer blend electrospun sample (ES ATQ/VA:K90 1:1) showed continuous

dissolution enhancement. The advantage of hydrophilic-hydrophobic balance optimisation further affects the *ex vivo* permeation profiles. Physical mixture and electrospun of ATQ/VA:K90 1:1 showed the shortest lag time in achieving quantifiable permeated ATQ concentration through porcine buccal skin in comparison to other polymeric compositions. Further investigation on the storage stability of electrospun samples revealed dry and temperate conditions maintained the sample amorphicity and exerted a beneficial impact in sustaining the supersaturation state. Ageing in a dry storage condition prevented moisture-induced recrystallisation and allowed stabilisation of the amorphous sample to its equilibrium glassy state through structural relaxation. Unlike the fresh product, dissolution of the aged product showed that the formulation containing only hydrophilic components in carrier matrix (ES ATQ/K90) revealed a more prominent beneficial impact in sustaining the supersaturation state over ageing comparing the other formulations with hydrophobic components. This serves as an option to sustain the supersaturation state achieved by amorphous solid dispersion apart from the optimisation of the hydrophilic-hydrophobic balance of the polymeric carrier system.

## CHAPTER 1

### INTRODUCTION AND LITERATURE REVIEW

#### 1.1 General Introduction

Atovaquone (ATQ) is a synthetic hydroxynaphthoquinone with broad-spectrum antiprotozoal activity. Currently, ATQ is used as a fixed-dose combination with proguanil (Malarone<sup>®</sup>) for the prophylaxis of malaria. Besides, Malarone<sup>®</sup> was listed for the treatment of uncomplicated malaria in travellers out of malaria-endemic regions. As an alternative treatment for uncomplicated malaria, Malarone<sup>®</sup> combination use with artesunate and primaquine was also suggested (WHO, 2015). Apart from the therapeutic effect in malaria prevention and treatment when ATQ was used in combination with proguanil, ATQ alone was utilised in the prevention and treatment of *pneumocystis carinii* pneumonia (PCP) (Baggish and Hill, 2002). It was concluded that when a sufficient level in blood was achieved, ATQ could act as an effective alternative to trimethoprim-sulfamethoxazole in PCP treatment (Baggish and Hill, 2002). In combination with azithromycin, ATQ was proved to show efficacy in treating babesiosis. Such a combination was identified to result in a comparable efficacy and fewer side effects than the standard quinine-clindamycin treatment (Krause et al., 2000). Concerning the efficacy of ATQ against other parasites, ATQ was also reported to be a promising alternative for toxoplasmosis treatment based on the results from clinical trials (Kovacs and The, 1992, Pearson et al., 1999). In recent years, ATQ was mentioned to have anticancer properties which further highlights the need for further scrutiny of the monotherapy usage of this drug. Particularly, the chemosensitivity of ATQ towards cell lines in eye cancer (Ke et al., 2018), brain

cancer (Takabe et al., 2018), breast cancer (Gupta and Srivastava, 2019), acute myeloid leukaemia (Stevens et al., 2019) and ovarian cancer (Guo et al., 2021) was reported.

Despite the clinical benefits of ATQ, the bioavailability of ATQ is limited at 23% and 47% in the commercially available tablet and suspension formulations respectively (GSK, 2016) due to its low aqueous solubility. In the context of drug delivery, the bioavailability of an active pharmaceutical ingredient (API) is dependent on its aqueous solubility and intestinal permeability as described in the Biopharmaceutics Classification System (BCS). According to the BCS provided by U.S. Food and Drug Administration (FDA), APIs are classified into four classes based on their aqueous solubility and intestinal permeability as shown in Table 1.1 (Amidon et al., 1995).

Table 1.1 Biopharmaceutics Classification System of API according to aqueous solubility and intestinal permeability

	High solubility	Low solubility
High permeability	Class I	Class II
Low permeability	Class III	Class IV

Low aqueous solubility is deemed to be a hurdle in drug absorption as the drug has to be dissolved prior to intestinal permeation. Atovaquone is categorised as Class II which renders its low bioavailability.

As a rule of thumb, altering the solubility will potentially improve the dissolution and ultimately bioavailability of a drug. Improvement of ATQ's solubility can be done through formulation strategy which is the main interest of the current study. The strategies to increase drug solubility include drug polymorphism, amorphisation and the additional of excipients to form solid dispersion (SD) are all closely related to the



physical state of the drug. The theoretical background of these aspects will be discussed in the subsequent sections of this chapter.

## 1.2 Atovaquone

The development of atovaquone (ATQ) originated from the research of lapachol derivatives (Wright, 2009) which aimed to tackle a substantial shortage in quinine supply for malaria treatment due to the outbreak of World War II (Nixon et al., 2013). Over decades of effort, the chemical synthesis of ATQ was first disclosed and patented in US patent no. 4981874 in 1991 (Latter and Gutteridge, 1991).

Figure 1.1 and Table 1.2 showed the molecular structure and physicochemical properties of ATQ. Further insight into the solid states of ATQ will be investigated in Chapter 3.

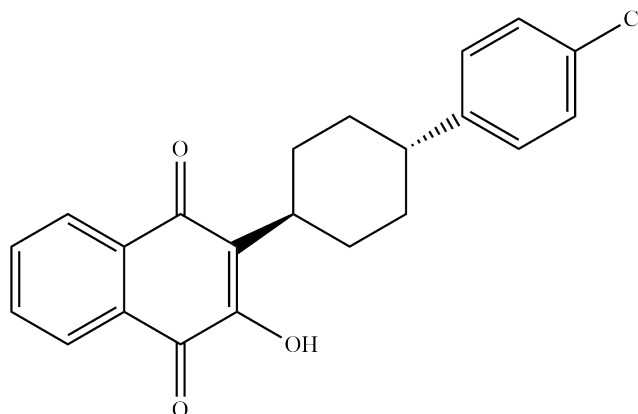


Figure 1.1 Molecular structure of ATQ

Table 1.2 Physicochemical properties of ATQ

Properties	ATQ	Reference
IUPAC chemical name	3-[4-(4-chlorophenyl)cyclohexyl]-4-hydroxynaphthalene-1,2-dione	(PubChem, 2022)
Formula	C <sub>22</sub> H <sub>19</sub> ClO <sub>3</sub>	(PubChem, 2022)
Molecular weight	366.837	(Nixon et al., 2013)
pKa	≈5.0 (calculated)	(Lindegarh et al., 2001)
Log P	5.80 (measured) 4.74 (predicted)	(Nixon et al., 2013)
Solubility in water (g/L)	Insoluble (measured) 7.96×10 <sup>-4</sup> (predicted)	(Nixon et al., 2013)
Plasma protein binding (%)	99.9	(Nixon et al., 2013)
Half-life (days)	2.2-3.2	(Nixon et al., 2013)

### 1.2.1 Safety and Toxicity

Generally, ATQ was reported to be well tolerated. The side effects of ATQ usage reported include nausea, vomiting, diarrhoea, rash, headache and fever (GlaxoSmithKline, 2013).

### 1.2.2 Pharmacokinetics Profile

Atovaquone is a highly lipophilic drug with low aqueous solubility, thus the bioavailability of ATQ is highly dependent on the formulation and diet. It was reported that the suspension formulation (Mepron<sup>®</sup>) provides about a two-fold increment in ATQ bioavailability compared to the tablet formulation (Malarone<sup>®</sup>) under the same fasting or fed conditions. Based on the product monograph, the absolute bioavailability of suspension and tablet under fed conditions was 47 ± 15% and 23 ± 11% respectively (GlaxoSmithKline, 2013).

Atovaquone shows high plasma protein binding (99.9%) and a volume of distribution around 7.98 L/kg. The metabolism of ATQ in humans remains unknown (Nixon et al., 2013). Elimination of ATQ is mainly through the liver with more than 90% of ATQ excreted in bile in its parent form. A possibility of enterohepatic recirculation of ATQ was highlighted as the pharmacokinetic profile shows a reduction followed by an increase in drug concentration over time (Nixon et al., 2013).

### **1.3 Solid-State Forms**

Pharmaceutical materials can exist in distinct solid states, i.e., the ordered crystalline state and disordered amorphous state (Byrn et al., 2017c). In the crystalline state, a compound may present more than one possible crystalline phase which is known as polymorphs. This phenomenon is named polymorphism (further described in Section 1.3.1(a)). The difference in crystalline structural arrangement affects the physicochemical properties of the materials such as density, solubility, melting point and chemical stability due to the existence of different intermolecular and intramolecular interactions (Hilfiker et al., 2006). When solvent molecules are introduced to the crystal lattice, a pseudopolymorph known as solvate forms. A solvate is named hydrate when the introduced solvent is water. The introduction of non-volatile molecules to the crystal lattice leads to the formation of co-crystals. Both solvates and co-crystals may exist in various polymorphs. By interacting an acidic/basic compound with a suitable base/acid, a salt is formed as a result of recrystallisation. The formed crystalline salts may also exist in various polymorphs and solvates (Hilfiker et al., 2006). Figure 1.2 illustrates the solid-state forms of a material.

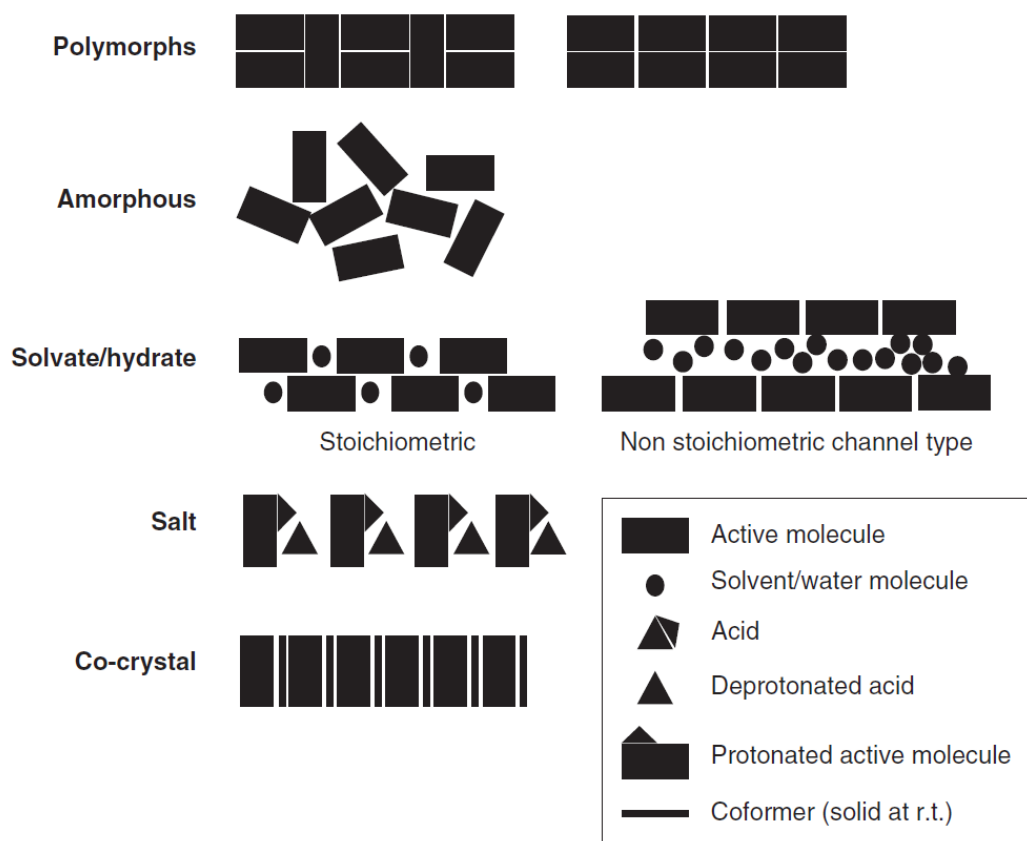


Figure 1.2 Schematic illustration of different states of solid material. This figure is adapted from Hilfiker et al. (Hilfiker et al., 2006).

### 1.3.1 Crystalline Materials

Generally, crystalline materials have a regular molecular arrangement with long-range order (Byrn et al., 2017c). A crystal shows a lower enthalpy and specific volume as compared to its corresponding amorphous form, indicating that the crystal is thermodynamically more stable (Yu, 2001). Frequently, polymorphism was reported to occur in crystalline compounds (Karpinski, 2006).

### 1.3.1(a) Polymorphism

In the pharmaceutical field, it has been reported that 50% of APIs show polymorphic forms (Karpinski, 2006). Polymorphs have been described as containing the same chemical composition but differing in the internal structures including the unit cell dimension, crystal packing and molecular conformation. From the structural aspect, polymorphs have been classified into two categories, i.e., configurational polymorphs and conformational polymorphs (Byrn et al., 2017b).

In general, configurational polymorphs occur in molecules that are relatively rigid in their conformation. Configurational polymorphs show an identical molecular conformation but differ in their packing motif and molecular interaction pattern (Byrn et al., 2017b). Such a mechanism is termed packing/configurational polymorphism. An example of configurational polymorphism was reported in carbamazepine. Based on the literature, carbamazepine shows four polymorphs (Grzesiak et al., 2003, Lowes et al., 1987, Himes et al., 1981, Lang et al., 2002). All four carbamazepine polymorphs show similar molecular conformation with strong hydrogen bonding of anticarboxamide dimers. However, they differ in the packing of dimer units. Form I exists in triclinic (Grzesiak et al., 2003), form II in trigonal (Lowes et al., 1987), form III in primitive monoclinic (Himes et al., 1981) and form IV in face-centred monoclinic (Lang et al., 2002) crystal system. The difference in crystal packing leads to the variation in structure internal energy and stability. It was reported that the stability of carbamazepine at room temperature is form III > form I > form IV > form II (Grzesiak et al., 2003).

On the other hand, conformational polymorphs occur in molecules with flexible structures which form several conformations and are later packed into other crystal phases (Byrn et al., 2017b). For instance, ritonavir shows conformational polymorphism (Bauer et al., 2001). Ritonavir form I exist in the ‘cis’ conformation while form II exists in the ‘trans’ conformation. Apart from the conformational difference, the polymorphs show distinctive morphology, crystal packing and hydrogen bonding (Bauer et al., 2001).

Although polymorphs could be generally classified as configurational polymorphs or conformational polymorphs based on their structural aspects, the distinction between the two types of polymorphisms remains unclear. Packing motifs and conformations of molecules are generally interrelated and subsequently affect molecular interactions such as hydrogen bonding. Variation in packing, conformation and interaction leads to the formation of crystal structures with distinct physical properties. Table 1.3 shows the physical properties that may vary in different polymorphs.

Table 1.3 Physical properties variation in polymorphs (Byrn et al., 2017b)

<b>Types of Physical Properties</b>	<b>Description</b>
Packing	Molar volume Density Electrical conductivity Thermal conductivity Hygroscopicity
Thermodynamic	Melting temperature Sublimation temperature Internal energy Enthalpy Heat capacity Entropy Free energy and chemical potential Thermodynamic activity Vapour pressure Solubility
Spectroscopic	Electronic transition Vibrational transition Rotational transition Nuclear spin transition
Kinetic	Dissolution rate Rates of solid-state reactions Stability
Surface	Surface free energy Interfacial tension Habit
Mechanical	Hardness Tensile strength Compactibility, tableting Handling, flow and blending

### 1.3.1(b) Thermodynamic Stability of Polymorphs

Gibbs free energy is commonly utilised to determine the relative stability of polymorphs where a more stable polymorph has lower free energy. The individual polymorph is considered the thermodynamically stable polymorph when it has the lowest free energy at the defined environmental temperature and pressure (except at the transition point). In the same condition, the rest of the polymorphic forms are considered to be metastable forms. A metastable polymorph is thermodynamically

unstable and hence the existence period is highly dependent on the transformation kinetics. In the situation where the metastable polymorph shows slow transformation kinetics, it could be kinetically stable at storage for years (Byrn et al., 2017b).

Two types of stability, i.e., monotropy and enantiotropy are used to describe a pair of polymorphs. At a temperature below the melting point, a monotropic pair remains the same relative stability. Based on Figure 1.3(left), form A and form B intersect with the liquid phase at their respective melting points ( $T_{m,A}$  and  $T_{m,B}$ ).

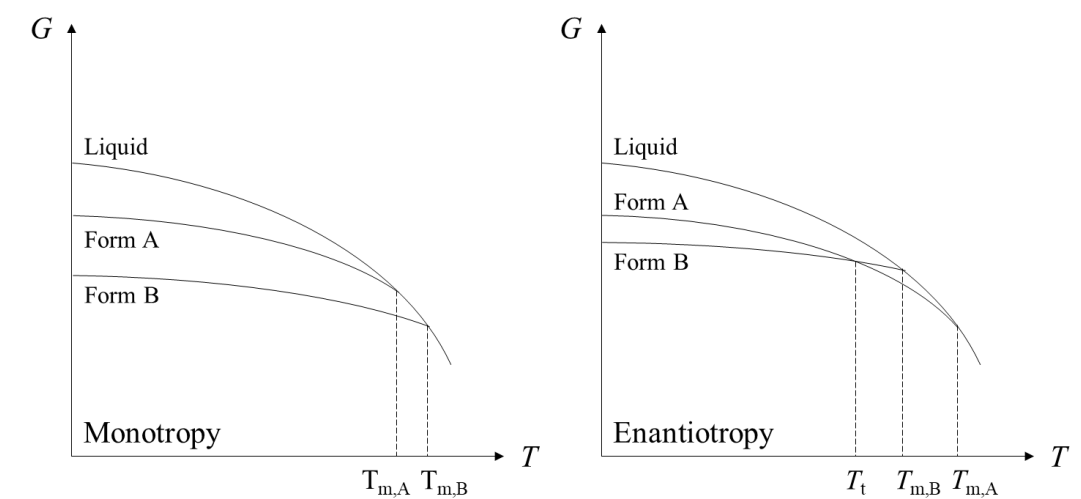


Figure 1.3 Relationship between Gibbs free energy and temperature for monotropic and enantiotropic polymorph pair. This figure is adapted and modified from Byrn et al. (Byrn et al., 2017b)

At the melting point, the crystal is at an equilibrium state with the liquid phase with zero  $\Delta G$ . Considering the polymorphs are a monotropic pair, form B is identified as the stable form as it has a lower Gibbs free energy compared to form A below the melting point. Therefore, a thermodynamic tendency for form A to transform to form B is possible since  $\Delta G < 0$ . However, it would be hard to observe the transformation of monotropic pairs in the solid-state due to the significant kinetic barrier. Instead, the



polymorphic change could happen in a suspension system via the solution-mediated transformation (Byrn et al., 2017b).

In the enantiotropic system as shown in Figure 1.3(right), the stability of polymorph changes above and below the transition temperature ( $T_t$ ) as the  $T_t$  appears before the melting temperatures ( $T_{m,A}$  and  $T_{m,B}$ ). At a temperature below  $T_t$ , form B is considered the more stable form while form A is considered the more stable form when the applied temperature exceeds  $T_t$  (Byrn et al., 2017b). The relative stability of polymorphs becomes complicated when a compound exists with more than two polymorphs.

To categorise the polymorphic pair into either monotropic or enantiotropic, Bruger and Ramberger's rules which comprise the heat of transition rule, the heat of fusion rule and the density rule are considered (Burger and Ramberger, 1979). According to the heat of transition rule, two polymorphs are categorised as a monotropic pair when an exothermic transition occurs at a particular temperature and no transition happens at a higher temperature. An enantiotropic pair shows an endothermic transition at a particular temperature with the  $T_t$  below that temperature (Burger and Ramberger, 1979).

The heat of fusion rule describes two polymorphs to be a monotropic pair when the polymorph with a higher melting point has a higher heat of fusion. Contrastingly, enantiotropic pairs are identified when the polymorph with a higher melting point has a lower heat of fusion (Burger and Ramberger, 1979).

The density rule applies to determine the relative stability of polymorphs that have van der Waals interactions dominating their crystal packing. In such a system, a polymorph with the highest density is recognised to be the stable form (Burger and Ramberger, 1979). For instance, the stable nabumetone form I has a higher density ( $1.26 \text{ g/cm}^3$ )

than its corresponding metastable form II (1.21 g/cm<sup>3</sup>) (Price et al., 2002). When hydrogen bonding is the dominant interaction within the system, the most stable form shows a lower density. For example, the stable ritonavir form II has a lower density (1.25 g/cm<sup>3</sup>) than its corresponding metastable form I (1.28 g/cm<sup>3</sup>) (Bauer et al., 2001).

### **1.3.1(c) Polymorph Conversion**

As the kinetic process was mentioned to affect the stability and existence period of a metastable polymorph, an understanding of the kinetic mechanism is crucial. The kinetic mechanism in the solid states would be expected to differ from that in the solution condition.

In the solution condition, three steps, i.e., dissolution of the metastable polymorph, nucleation of stable polymorph and growth of the stable polymorph are involved in the polymorph conversion. This phenomenon is named solution-mediated transformation. It is generally observed that the metastable polymorph possesses a higher solubility than the stable form. Subsequently, nucleation and growth of the stable form occur (Byrn et al., 2017b).

The polymorphic transformation in the solid-state is more complex than the solution-mediated transformation as the mechanism involved remains unclear. To initiate the solid-state polymorph conversion, activation energy needs to be overcome. The activation energy of a system could be affected by the crystal packing, particle size, defects, impurities, temperature and humidity (Byrn et al., 2017b). A high temperature is often reported to accelerate the transition of metastable polymorph to stable polymorph (Byrn et al., 2017b). For instance, the R form (a metastable polymorph of

ROY) transforms into the OP and Y forms after years of storage at room temperature. In contrast, the R form changes to Y, OP and ON forms within hours to days at an elevated temperature of 70-100°C (Yu et al., 2000). High temperature increases molecular mobility and subsequently initiates transformation at the defect sites. As the molecules at the defects sites are high in energy, nucleation and growth of a new phase occur. Besides, structural similarity between the polymorphs affects the activation energy for nucleation. A slow transformation occurs in the system which requires high activation energy to reorganise and restructure into a new phase. Contrastingly, when polymorphs are highly similar in their conformation and packing pattern, a rapid conversion is possible as low energy is required to initiate changes in the parent species (Byrn et al., 2017b).

### **1.3.2 Amorphous Materials**

In contrast to crystalline materials, amorphous materials have an irregular molecular arrangement with short-range order (Byrn et al., 2017c). Owing to the lack of crystal lattice and strong lattice energy within the structure, an amorphous material shows an enhanced apparent solubility in an aqueous solution and subsequently enhanced bioavailability of the compound (Hancock and Parks, 2000). Therefore, amorphisation has been seen to be useful in overcoming the issue of poorly aqueous soluble crystals.

However, an amorphous exhibits a higher enthalpy and specific volume as compared to its corresponding crystalline structure, thus behaving thermodynamically metastable. (Yu, 2001). Due to the physical instability of the amorphous system, solid-state reversion to its stable crystalline system over a storage period would be possible. Therefore, it is important to identify the strategies for maintaining/enhancing the stability of an amorphous system.

### **1.3.2(a) Formation of Amorphous Solids**

To understand the formation of amorphous solids, the relationship of Gibbs free energy and temperature between the crystalline and liquid form of a molecule is considered. Based on Figure 1.4A, an API exists as a solid with lower free energy than liquid form at temperatures below the melting point ( $T_m$ ). Hence, the solid API is in a thermodynamically stable state. As the temperature increases above  $T_m$ , the solid API melts into liquid form and remains at a lower free energy level. A gradual decrease in temperature below  $T_m$  restores the crystallinity of the API through the formation of crystal nuclei and subsequent crystallisation. Crystallisation is an exothermic process where a sudden contraction of the system occurs. As a result, both enthalpy and volume of the system decrease at  $T_m$  as shown in Figure 1.4B.

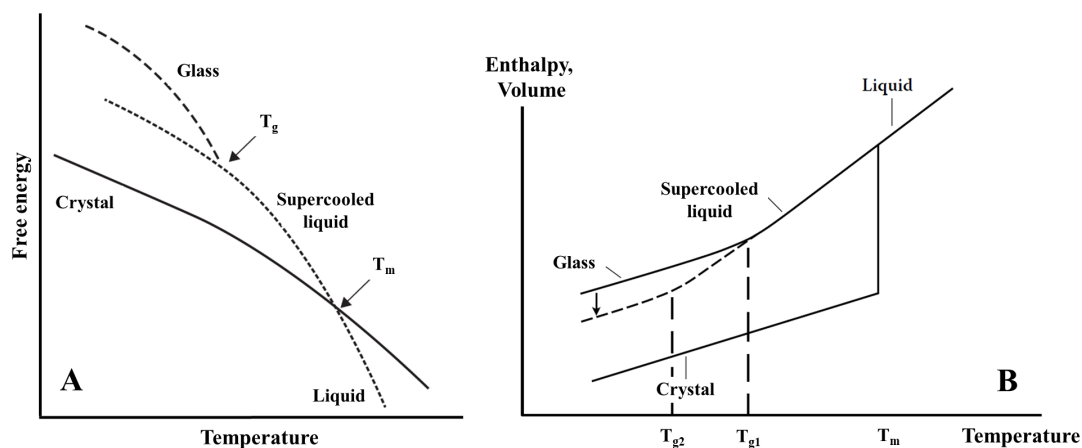


Figure 1.4 (A) Plot of Gibbs free energy against the temperature of a material at its respective equilibrium and non-equilibrium states. This figure is adapted and modified from Byrn et al. (Byrn et al., 2017a). (B) Plot of enthalpy and volume against the temperature of a material at its respective state transition (crystallization or glass transition). This figure is adapted and modified from Reading and Craig (Reading and Craig, 2007)

In contrast, a rapid cooling below  $T_m$  produces supercooled liquid. At this state, the supercooled liquid behaves metastable relative to the crystal counterpart. It was noted that supercooled liquid maintains an equilibrium state as the liquid form. Further decrease in temperature leads to the achievement of a non-equilibrium state, forming an unstable glassy solid at the glass transition temperature,  $T_g$  (further described in Section 1.3.2(c)).

### 1.3.2(b) Preparation of Amorphous Solids

Referring to the previous section (Section 1.3.2(a)), an amorphous solid can be prepared by rapid cooling of crystal melt where recrystallisation is completely avoided. Apart from the melt quench method, several methods, i.e., introduction of sufficient energy to break crystal lattice into disordered amorphous form and allowing API

molecules to be at a highly disordered state which prevents crystallisation could produce amorphous solids. Table 1.4 lists the methods utilised in preparing pharmaceutical amorphous solids.

Table 1.4 Preparation of amorphous solids (Byrn et al., 2017a, Newman, 2015)

<b>Method</b>	<b>Sample Form</b>	<b>Example</b>
Lattice disruption	Crystal	Milling Roller compaction Tablet compaction Irradiation Desolvation of solvate and hydrate
Melt quench	Liquid melt	Melt extrusion
Condensation	Vapour	Sublimation
Solvent removal	Solution	Freeze drying (lyophilisation) Rotary evaporation Spray drying Electrospinning Aqueous film coating/film preparation Wet granulation

According to the literature, the production of amorphous solids through an introduction of sufficient energy to disrupt the crystal lattice is evident. For instance, a reduction in the crystallinity of indomethacin was reported as grinding time increased (Bates et al., 2006). Lattice disruption could also be done through the removal of organic solvents/water from solvate/hydrate (Guo et al., 2000, Bates et al., 2007). As solvent is removed from the crystal lattice structure, the remaining crystal lattice becomes less dense and collapses, thus transforming the crystal into an amorphous form.

Similar to the theory behind the melt quench method, the preparation of an amorphous solid via condensation requires a highly disordered starting material (vapour) to be cooled below the melting temperature of the crystal (Byrn et al., 2017a). Also, crystallisation needs to be avoided by modifying the condensation rate to produce an amorphous solid.

Besides, the solvent removal method could be employed to produce amorphous solids from highly disordered molecules in solution form. The key to preparing amorphous solids from solution is rapid precipitation during the drying process to avoid the formation of crystalline counterparts via solvent-mediated crystallisation (Byrn et al., 2017a).

### **1.3.2(c) Glass Transition Temperature**

Referring to Section 1.3.2(a), an amorphous solid (also known as glassy solid) forms when supercooled liquid is further cooled to glass transition temperature ( $T_g$ ). As temperature decreases, the viscosity of the liquid increases, thus molecular mobility of the material decreases, representing a kinetic transition event. At  $T_{g1}$ , when the supercooled liquid cooled to a frozen state, the translational and rotational motions of the molecules were reduced. Upon continuous cooling to below  $T_{g1}$ , a glassy solid forms whereby only molecular vibrations are present. The  $T_g$  value of an amorphous material is dependent on the rate change in temperature and the ability of supercooled liquid in the remaining equilibrium state. For instance, a slower cooling rate results in the formation of glassy solids with a lower  $T_g$  ( $T_{g2}$  as presented in Figure 1.4B). A slower cooling rate provides the viscous liquid a longer time to achieve equilibration, leading to the formation of glassy solids with a lower enthalpy, entropy and specific volume.

Interestingly, a different review on glass transition has been concluded by Suga (Suga, 2003). Regardless of the structural regularity, the aforementioned glass transitions which are typically observed in liquids was reported to occur in condensed state materials. A freezing-in phenomenon was proposed to occur in certain orientationally

disordered crystals and liquid crystals (either in a metastable or stable state) (Suga, 2003). Materials which undergo frozen-in disorder are thereby termed glassy crystals. Glassy crystals such as thiophene, ethanol and cyclohexanol were proved to show an apparent orientational glass transition in their thermal profile (Suga, 2003).

In general, the molecules are thermodynamically unstable in the glassy state and physical ageing of the glassy solid would be probable. Upon storage at a temperature below  $T_g$  over a measurable period, a decrease in molar volume and enthalpy of glassy solid could be observed (Byrn et al., 2017a).

### 1.3.2(d) Fragility

Fragility is defined by Angell in a plot of viscosity variations with temperature in Arrhenius form (Figure 1.5) (Angell, 1995).

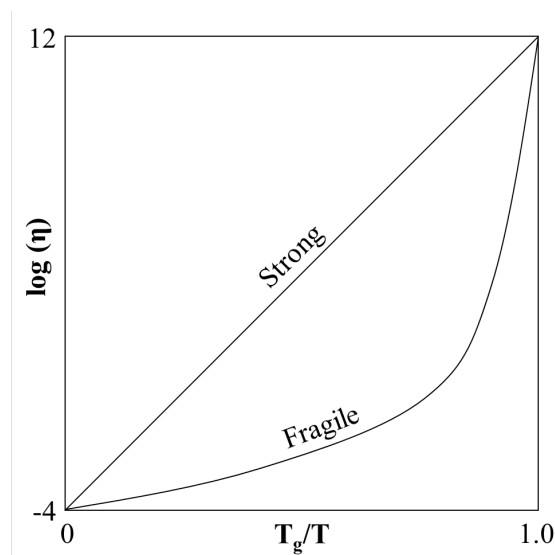


Figure 1.5 Simplified fragility schematic plot defined by Angell (Angell, 1995)



As shown in the plot (Figure 1.5), it was reported that some liquids showed a linear relationship and some showed deviation from the linearity of the Arrhenius equation (Equation 1.1).

$$\eta = K e^{\frac{-Ea}{RT}}$$

Equation 1.1

where  $\eta$  is viscosity,  $K$  is a constant,  $Ea$  is the activation energy of melt flow,  $R$  is the universal gas constant and  $T$  is the temperature (DiNunzio et al., 2010). It was suggested that the system which showed a linear relation in the Arrhenius plot is classified as a strong liquid while those which deviated from the linearity of the Arrhenius plot as a fragile liquid (Angell, 1995).

The fragility of an amorphous material is described by the fragility index,  $m$ , which can be derived from the  $T_g$  values from different heating/cooling rates of Differential Scanning Calorimetry scan by using Equation 1.2 and Equation 1.3,

$$m = \frac{\delta \log \tau}{\delta (T_g - T)}$$

Equation 1.2

$$m = \frac{\Delta E_{T_g}}{2.303 \times RT_g}$$

Equation 1.3

where  $\delta$  indicates the derivative function of Equation 1.2,  $\Delta E_{T_g}$  is the activation energy for structural relaxation at  $T_g$ ,  $\tau$  is relaxation time and  $R$  is the universal gas constant.  $\Delta E_{T_g}$  can be obtained from heating/cooling rate dependent on calorimetric  $T_g$  as described in Equation 1.4 (Moynihan et al., 1976).

$$\frac{d(\ln q)}{d\left(\frac{1}{T_g}\right)} = \frac{-\Delta E_{T_g}}{R}$$

Equation 1.4

By identifying the magnitude of the fragility index, an amorphous material could be categorised into a strong liquid when  $m < 40$  and a fragile liquid when  $m > 75$ . Those which lie in between are known as an intermediate fragile liquid (Yu, 2001). The value of the fragility index can be further used to reflect the physical stability of an amorphous system.

In the pharmaceutical field and final product development, the advantages of amorphous material could be potentiated using SD as the formulation strategy which will be introduced in the following section.

#### **1.4 Solid Dispersion**

The application of SD was first described by Sekiguchi and Obi in 1961. They reported that a eutectic mixture improves the rate of drug release and hence the bioavailability of the poorly aqueous soluble API (Sekiguchi and Obi, 1961). In 1971, Chiou and Riegelman defined SD as the dispersion of one or more APIs in an inert carrier at a solid state via the melting, solvent or melting-solvent methods (Chiou and Riegelman, 1971). To date, SD has been applied in the pharmaceutical industry and products have been commercially available as listed in Table 1.5.

Table 1.5 Commercially available FDA-approved solid dispersion products

Year	Tradename	Drug	Excipient	Manufacturing Method	Dosage Form	Trademark Owner
1982	Gris-PEG <sup>®</sup>	Griseofulvin	PEG 400/PEG 8000/PVP	Melting	Tablet	Bausch Health (Valeant)
1985	Cesamet <sup>®</sup>	Nabilone	PVP	Unknown	Capsule	Bausch Health (Valeant)
1992	Sporanox <sup>®</sup>	Itraconazole	HPMC/PEG 20000	Unknown	Capsule	Janssen
1994	Prograf <sup>®</sup>	Tacrolimus	HPMC	Unknown	Capsule	Astellas
2003	Crestor <sup>®</sup>	Rosuvastatin	PVP/HPMC	Unknown	Tablet	AstraZeneca
2004	Cymbalta <sup>®</sup>	Duloxetine	HPMC/HPMC-AS	Unknown	Capsule	Eli Lilly
2004	Palladone <sup>™</sup>	Hydromorphone hydrochloride	Ethylcellulose	HME	Capsule	Purdue Pharma
2005	Kaletra <sup>®</sup>	Lopinavir/Ritonavir	PVP/HPMC/HPC/PEG 400/PEG 3350	HME	Tablet	Abbvie
2007	Fenoglide <sup>®</sup>	Fenofibrate	PEG 6000/poloxamer 188	Melting	Tablet	Salix
2008	Intelence <sup>®</sup>	Etravirine	HPMC	Spray drying	Tablet	Janssen
2008	Nucynta <sup>®</sup>	Tapentadol	PVP	HME	Tablet	Janssen
2009	Afinitor <sup>®</sup>	Everolimus	PVP/HPMC	Spray drying	Tablet	Novartis
2009	Ozurdex <sup>®</sup>	Dexamethasone	PLGA	HME	Intravitreal implant	Allergan
2009	Samsca <sup>®</sup>	Tolvaptan	HPC	Granulation	Tablet	Otsuka America
2010	Norvir <sup>®</sup>	Ritonavir	PVP/HPC/HPMC/PEG 400/PEG 3350	HME	Tablet	Abbvie
2010	Onmel <sup>®</sup>	Itraconazole	PVP/HPMC	Unknown	Tablet	Sebela (Merz Pharma)
2010	Zortress <sup>®</sup>	Everolimus	PVP/HPMC	Spray drying	Tablet	Novartis
2011	Nucynta <sup>®</sup> ER	Tapentadol	$\alpha$ -tocopherol/HPMC/PEG/PEO	HME	Tablet	Janssen
2011	Zelboraf <sup>®</sup>	Vemurafenib	HPMC-AS	Co-precipitation	Tablet	Hoffmann

Table 1.5 – continued

2012	Kalydeco <sup>®</sup>	Ivacaftor	HPMC-AS/PEG 3350/PVA	Spray drying	Tablet	Vertex
2012	Stivarga <sup>®</sup>	Regorafenib	PVP	Granulation	Tablet	Bayer
2013	Astagraf XL <sup>®</sup>	Tacrolimus	HPMC	Unknown	Capsule	Astellas
2013	Noxafil <sup>®</sup>	Posaconazole	HPMC-AS/HPC/PVA/PEG 3350	HME	Tablet	Merck
2014	Belsomra <sup>®</sup>	Suvorexant	Copovidone	HME	Tablet	Merck
2014	Viekira Pak <sup>®</sup>	Ombitasvir/Paritaprevir/ Ritonavir/Dasabuvir	Copovidone/TPGS/propylene glycol monolaurate type I	HME	Tablet	Abbvie
2015	Envarsus <sup>®</sup>	Tacrolimus	HPMC/PEG/poloxamer	Melt granulation	Tablet	Veloxis
2015	Orkambi <sup>®</sup>	Ivacaftor/Lumacaftor	HPMC-AS/PVP/SLS	Spray drying, wet granulation	Tablet	Vertex
2015	Technivie <sup>™</sup>	Ombitasvir/Paritaprevir/ Ritonavir	Copovidone/TPGS/propylene glycol monolaurate type I	HME	Tablet	Abbvie
2016	Venclexta <sup>®</sup>	Venetoclax	Copovidone	HME	Tablet	Abbvie
2016	Zepatier <sup>®</sup>	Elbasvir/Grazoprevir	PVP/HPMC/SLS/TPGS	Spray drying	Tablet	Merck
2017	Mavyret <sup>®</sup> Maviret <sup>®</sup>	Glecaprevir/Pibrentasvir	TPGS/propylene glycol monocaprylate (PGMC II)/ Copovidone	HME	Tablet/oral pellets	Abbvie
2018	Erleada <sup>®</sup>	Apalutamide	HPMC-AS	Spray drying	Tablet	Janssen
2018	Lynparza <sup>®</sup>	Olaparib	Copovidone	HME	Tablet	AstraZeneca
2018	Orilissa <sup>™</sup>	Elagolix	Pregelatinised starch/PVP/PVA/PEG	Wet granulation	Tablet	Abbvie
2019	Symdeko <sup>®</sup>	Tezacaftor/Ivacaftor	HPMC/HPMC-AS/SLS	Spray drying	Tablet	Vertex
2019	Trikafta <sup>®</sup>	Elexacaftor/Tezacaftor/Ivacaftor	HPMC/HPMC-AS/SLS	Spray drying	Tablet	Vertex
2020	Braftovi <sup>®</sup>	Encorafenib	Copovidone/poloxamer/crospovidone	HME	Capsule	Pfizer
2020	Oriahnn <sup>®</sup>	Elagolix/Estradiol/Noret hindrone acetate	PEG/crospovidone/PVA/PEG/copovidone/ HPMC	HME	Capsule	Abbvie

### **1.4.1 Classification of Solid Dispersion**

Solid dispersion development is classified into four generations as described below.

#### **1.4.1(a) First Generation of Solid Dispersion**

In the early phase of SD development, crystalline carriers such as urea (Sekiguchi and Obi, 1961, Sekiguchi et al., 1964, Goldberg et al., 1966) and sugar (Kanig, 1964) were employed. The produced SD showed a faster drug release compared to the conventional formulations mainly due to the reduction of drug particle size. However, the developed crystalline SD is thermodynamically stable and generally shows a slower drug release than its amorphous counterparts.

#### **1.4.1(b) Second Generation of Solid Dispersion**

In the second generation of SD, amorphous carriers were utilised to produce SD. Polymeric carriers such as PVP (Simonelli et al., 1969), PEG (Urbanetz, 2006), HPMC (Ohara et al., 2005) and cyclodextrin (García-Zubiri et al., 2006) were incorporated. As a result, the achievement of supersaturation (Urbanetz, 2006), reduction of drug particle size at the molecular level and production of amorphous SD were demonstrated success (van Drooge et al., 2006).

#### **1.4.1(c) Third Generation of Solid Dispersion**

The formulation of SD was later improved in the third generation by utilising surfactant, a mixture of polymers and a mixture of surfactant-polymer as the carrier systems. The third generation SD was designed to stabilise the dispersed system by avoiding amorphous drugs from recrystallisation, consequently achieving the highest degree of bioavailability of poorly soluble APIs (Vasconcelos et al., 2007). For instance, surfactants such as gelucire 44/14 (Damian et al., 2000), poloxamer (Majerik et al., 2007) and inulin (van Drooge et al., 2006) were utilised.

#### **1.4.1(d) Fourth Generation of Solid Dispersion**

The fourth generation of SD aims to produce formulations with extended and controlled release profiles besides improving the solubility of poorly soluble APIs with a short biological half-life (Kaushik et al., 2020). Both aqueous soluble and insoluble carrier systems are applied in the formulation of the fourth generation SD (Tekade and Yadav, 2020). The aqueous soluble carrier helps to improve the solubility while the insoluble/slowly dissolving/swellable carrier is responsible to prolong the release in a controlled manner (Alshehri et al., 2020).

#### **1.4.2 Types of Solid Dispersion**

Solid dispersion is further categorised into two types, namely non-molecular and molecular dispersions as detailed below.